Chinese Journal of Physics 81 (2023) 303–324

Contents lists available at ScienceDirect

Chinese Journal of Physics

journal homepage: www.sciencedirect.com/journal/chinese-journal-of-physics

Stability, electronic band structure, magnetic, optical and thermoelectric properties of CoXCrZ (X = Fe, Mn and Z = Al, Si) and FeMnCrSb quaternary Heusler

K. Bouferrache [a,b], M.A. Ghebouli [c,d], B. Ghebouli [f], M. Fatmi [c,*], Sultan Alomairy [e], T. Chihi [c]

[a] Department of Physics, Faculty of Science, University of of Mohamed Boudiaf, M'sila, 28000, Algeria
[b] Laboratory of Physics and Chemistry of Materials, University of Mohamed Boudiaf, M'sila, 28000, Algeria
[c] Research Unit on Emerging Materials (RUEM), University Ferhat Abbas of Setif 1, Setif, 19000, Algeria
[d] Department of Chemistry, Faculty of Technology, University of Mohamed Boudiaf, M'sila, 28000, Algeria
[e] Department of Physics, College of Science, Taif University, P.O. Box 11099, Taif, 21944, Saudi Arabia
[f] Laboratory of Studies Surfaces and Interfaces of Solids Materials, Department of Physics, Faculty of Science, University Ferhat Abbas of Setif 1, Setif, 19000, Algeria

ARTICLE INFO

Keywords:
Heusler alloys
Half-metallic ferromagnetism
Thermoelectric
Spin gapless semiconductor
Spin polarization
Spintronics
Seebeck coefficient

ABSTRACT

Ab-initio simulations based on density functional theory as contained in the WIEN2k code using GGA, GGA+U, and mBJ approximations were used to perform the calculations. The energy of cohesion is minimal for FeMnCrSb, indicating that it is the most stable structure, with a lattice constant of 5.95 Å and 6.2184 Å for GGA and GGA+U. The ferromagnetic state is less stable than ferrimagnetic states in all studied quaternary Heusler. All the band structures are metallic, with the exception of the spin up case using GGA+U and mBJ approaches, where the semiconducting character is predicted. The amount of absorption and band gap validates the candidature of CoFeCrAl, CoFeMnSi, CoMnCrSi, and FeMnCrSb as absorber materials for photovoltaic devices. The high values of 0.8, 0.9, 0.95 and 1 for figure of merit (ZT) at 300 K were obtained for CoFeMnSi, CoFeCrAl, CoMnCrSi, and FeMnCrSb allowing their use in spintronic and thermoelectric applications. The resistivity of studied quaternary alloys is little sensitive to the temperature, while the electronic conductivity and power factor are proportional to the temperature.

1. Introduction

The usage of thermoelectric materials, which turn waste heat into electricity, is a part of the hunt for new ecologically friendly, renewable, and sustainable energy sources. The characteristics of Heusler alloys, such as their single electron spin polarization current, low lattice thermal conductivity, and high Seebeck coefficient, make them important materials [1–3]. Diverse physical properties such as HM magnets [4] that attracted spintronic device technologies. The electron-magnon interaction induces a finite density of states in the minority spin (spin down) band gap and results in spin Hall conductivity. Heusler quaternary alloys are magnetic intermetallics and crystallize in the cubic structure as LiMgPdSn prototype with (F-43m, No. 216) space group [5,6]. They exhibit desirable properties, such as robust spin polarization, semi-metallic magnetism, magnetoresistance, spin-free semiconductors, giant magnetocaloric and

* Corresponding author.
E-mail address: fatmimessaoud@yahoo.fr (M. Fatmi).

https://doi.org/10.1016/j.cjph.2022.10.003
Received 14 August 2022; Received in revised form 27 September 2022; Accepted 12 October 2022
Available online 13 October 2022

Table 1
The values of $R_{MT}xK_{max}$, R_{MT} of each constituent and k-point of CoFeCrAl, CoFeMnSi, CoMnCrSi and FeMnCrSb using GGA+U.

Heusler	Approach	$R_{MT}xK_{max}$	R_{MT} (X)	R_{MT} (X')	R_{MT} (Y)	R_{MT} (Z)	k-point
CoFeCrAl	**GGA+U**	9	1.9900	1.9000	1.8100	1.72	3000
CoFeMnSi	**GGA+U**	9	1.82	1.82	1.82	1.55	3000
CoMnCrSi	**GGA+U**	9	1.83	1.83	1.79	1.56	3000
FeMnCrSb	**GGA+U**	9	1.83	1.87	1.78	1.83	3000

Table 2
Configurations and atomic positions of the quaternary Heusler XX'YZ.

Configuration	X position	X' position	Y position
1	u	u	d
2	u	d	d
3	d	d	u
4	u	d	u
5	d	d	u
6	d	u	u
7	u	u	d
8	d	u	d

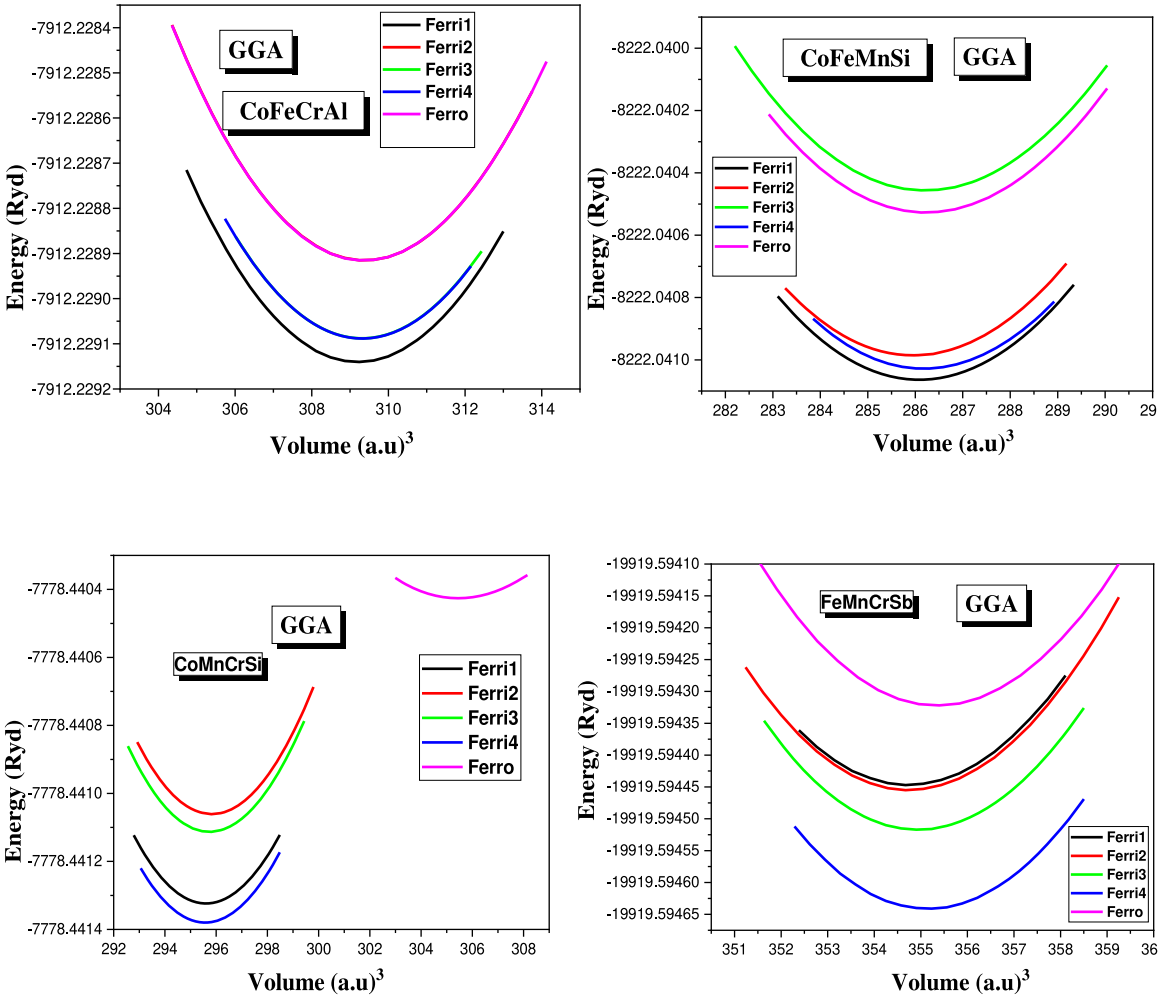

Fig. 1. The impact of volume on total energy for ferromagnetic and ferrimagnetic quaternary Heusler CoFeCrAl, CoFeMnSi, CoMnCrSi and FeMnCrSb in the GGA approximation.

Table 3
Equilibrium lattice constant, bulk modulus and its pressure derivative and cohesive energy of CoXCrZ (X = Fe, Mn and Z = Al, Si and Sb) and FeMnCrSb quaternary Heusler alloys calculated within GGA and GGA+U approximations.

Heusler	Parameters	GGA	GGA+U
CoFeCrAl	a (Å)	5.68	5.85
	B(GPa)	185.78	124.39
	B`	4.77	4.84
	E_{min} (Ry)	−7912.22	−7911.63
CoFeMnSi	a (Å)	5.33	5.77
	B(GPa)	252.44	132.25
	B`	5.2111	3.95
	E_{min} (Ry)	−8222.04	−8221.36
CoMnCrSi	a (Å)	5.59	5.7941
	B(GPa)	218.5	125.7
	B`	5.17	5.18
	E_{min} (Ry)	−7778.44	−7777.83
FeMnCrSb	a (Å)	5.94	6.2184
	B(GPa)	165.61	94.43
	B`	5.77	5.0908
	E_{min} (Ry)	−19919.59	−19919.02

thermoelectric effects. Spin electronics has led to a new class of semi-metallic ferromagnetic materials. One can make a ferromagnetic material from its non-magnetic constituents [7]. The adopted method resides on the doping of semiconductors with impurities of transition metals and non-magnetic elements [8,9]. Lakhan Bainsla et al. report the existence of spin gapless semiconductors behavior in the quaternary CoFeCrGa alloy, and transforms to half-metallic phase under pressure [10]. The resistivity of CoFeCrAl films is inversely proportional to the temperature, and the polycrystalline films have a coefficient of −0.19 cm/K, while the epitaxial films have a coefficient of −0.12 cm/K [11]. CoFeCrAl, CoFeMnSi, and CoFeMnGe Heusler alloys are spin gapless semiconductors [12], and the magnetoresistance of bulk CoFeCrAl is about 1.5% [13]. The ferromagnetic half-metals CoYMnGa and CoYMnAl [CoYMnGe and CoYFeZ (Z = Al, Si, Ge, and Ga)] by Heusler have a total magnetic moment of 4.00 B. (have no magnetic moment and are anti-ferromagnetic) [14]. The ferromagnetic quaternary Heusler CoYMnSi and CoYMnGe alloys have magnetic moments of 1.91 B and 2.90 B, respectively [14]. The spin gapless semiconductors (SGS) band structure is discovered to be present in several Heusler alloys; CoFeMnSi provides experimental support for this characteristic [15].

We studied in this work the LiMgPdSb-type quaternary Heusler alloys CoXCrZ (X = Fe, Mn and Z = Al, Si and Sb) and FeMnCrSb. In this work, we investigated the quaternary Heusler alloys CoXCrZ and FeMnCrSb of the LiMgPdSb type. The better magnetic, optical, and thermoelectric properties of the quaternary Heusler alloys under study in this work make them of great interest. The degree of structural organization and distribution of the atoms in the crystal lattice determine the electronic structure of Heusler alloys. The amount of absorption and band gap validates the candidature of CoFeCrAl, CoFeMnSi, CoMnCrSi, and FeMnCrSb as absorber materials for photovoltaic devices. The resistivity of studied quaternary alloys is little sensitive to the temperature, while the electronic conductivity and power factor are proportional to the temperature. The studied compounds had a small energy gap, which is one of the features interested in studying photovoltaic. The investigation of optical conductivity in the field 2 – 6 electron volts, and also the strong absorption for higher energy. We can consider these compounds as good within the energies shown in the figures and use them in solar panels.

2. Calculation model

The calculations were performed by employing the augmented plane-wave plus local orbitals basis functions as embodied in the WIEN2k code and GGA+U approximation [16]. The generalized gradient approximation (GGA) of Perdew, Burke and Ernzerhof is used as potential exchange-correlation in the calculation of the structural, magnetic and optical properties [17]. The electronic properties are determined using the modified Becke-Johnson approach [18]. The electron-electron correlation effect [19] is treated by the DFT+U approximation. The $R_{M.T}$ radius of Fe, Co, Mn, Cr, Si, Al and Sb are 1.24, 1.25, 1.24, 1.25, 1.16, 1.43 and 1.61 Å. The charge density and potentials are expressed using the spherical harmonic expansion with angular moments up to $I_{max} = 10$. We use the plane wave basis with cutoff of $R_{MT}xK_{max} = 9$. A mesh of 3000 k-points ensures convergence and overall energy minimization for the Brillouin zone integration. The valence and core states energy separation was fixed to - 8 Ry. 0.001 e was used for charge convergence. Our goal is to compare the results of various functionals because of the lack of experimental results. In this work, the Hubbard's coefficient was chosen U = 3 eV, and depends on the layer d. The RMT influences the electronic characteristics, but this effect is negligible compared to U and mBJ effects. The cohesive energy is an important physical quantity that accounts for the bond strength of a solid, which equals the energy needed to divide the solid into isolated atoms by breaking all the bonds. For unit cell of N atoms; the bulk cohesive energy per unit cell is [20]:

$$E_{coh}(\infty)\frac{E_{tot}(\infty)-\sum_N E_{iso}(\infty)}{N}$$

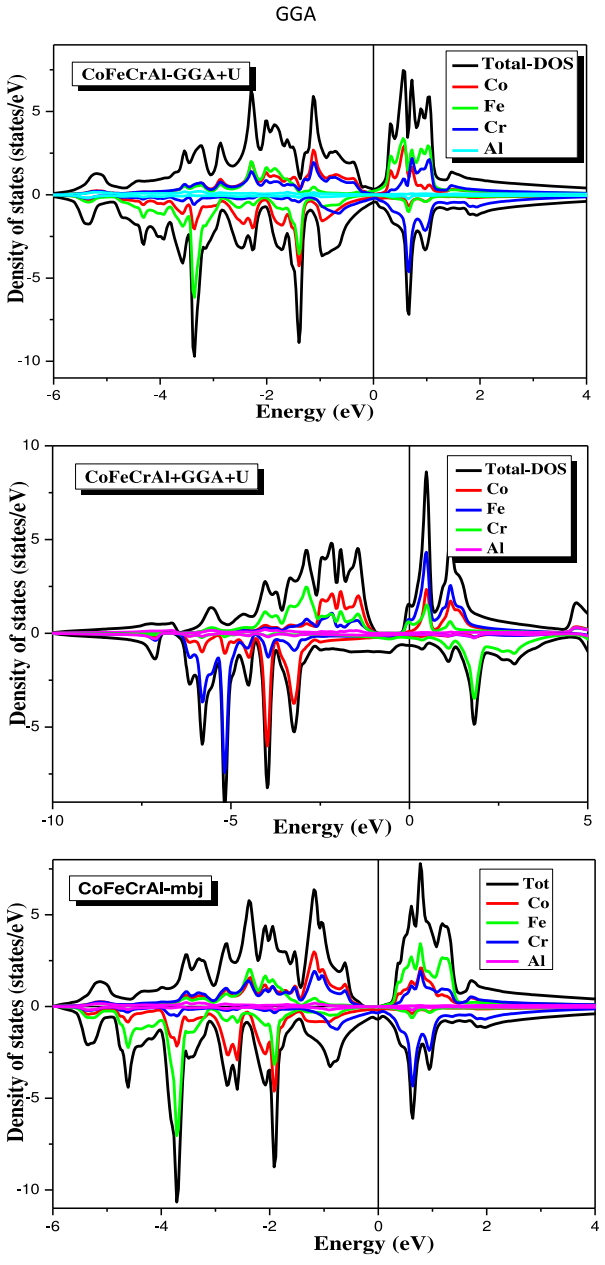

Fig. 2. The density of states for the quaternary Heusler CoFeCrAl computed by GGA, GGA+U and mBJ for spin up and spin down.

$$E_{coh}^{GGA}(r)\frac{E_{tot}^{GGA}(r)-\sum_{N}E_{iso}^{GGA}}{N}$$

GGA + U method corrects the formation energy and transition energy level. Lattice parameters, electrostatic potential, valence band maximum, transition energy level and total energy depend on the effective parameter (U_{eff}). For GGA + U_{eff}, when U_{eff} is taken as 3 eV, the calculated total energy is minimum.

3. Results and discussions

3.1. Stability

Quaternary Heusler CoXCrZ (X = Fe, Mn and Z = Al, Si and Sb) and FeMnCrSb have a LiMgPdSn-type structure, which crystallize into the face-centered cubic sublattices with F-43 m (No. 216) space group. The quaternary Heusler has the general form XX'YZ, where

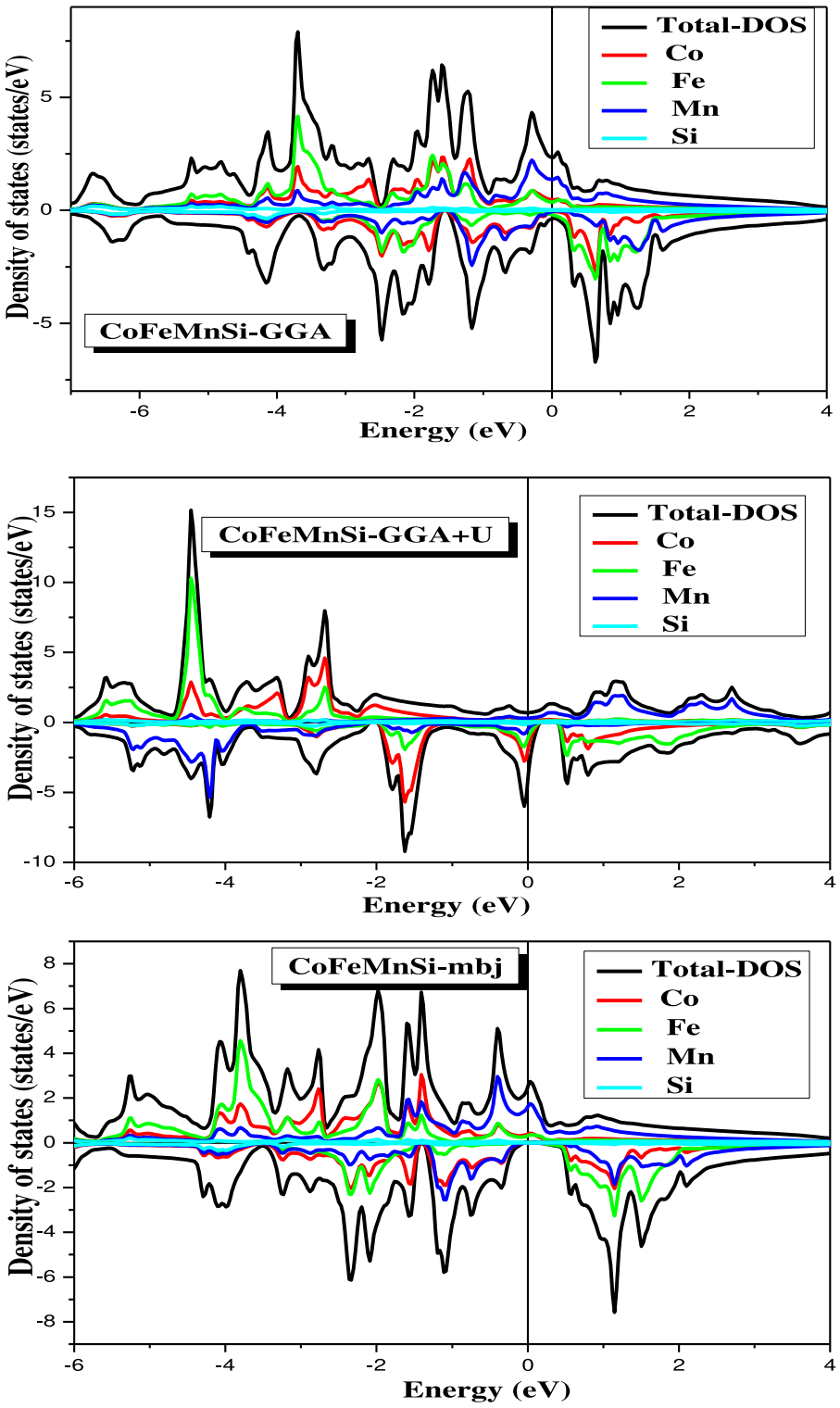

Fig. 3. The density of states for the quaternary Heusler CoFeMnSi computed by GGA, GGA+U and mBJ for spin up and spin down.

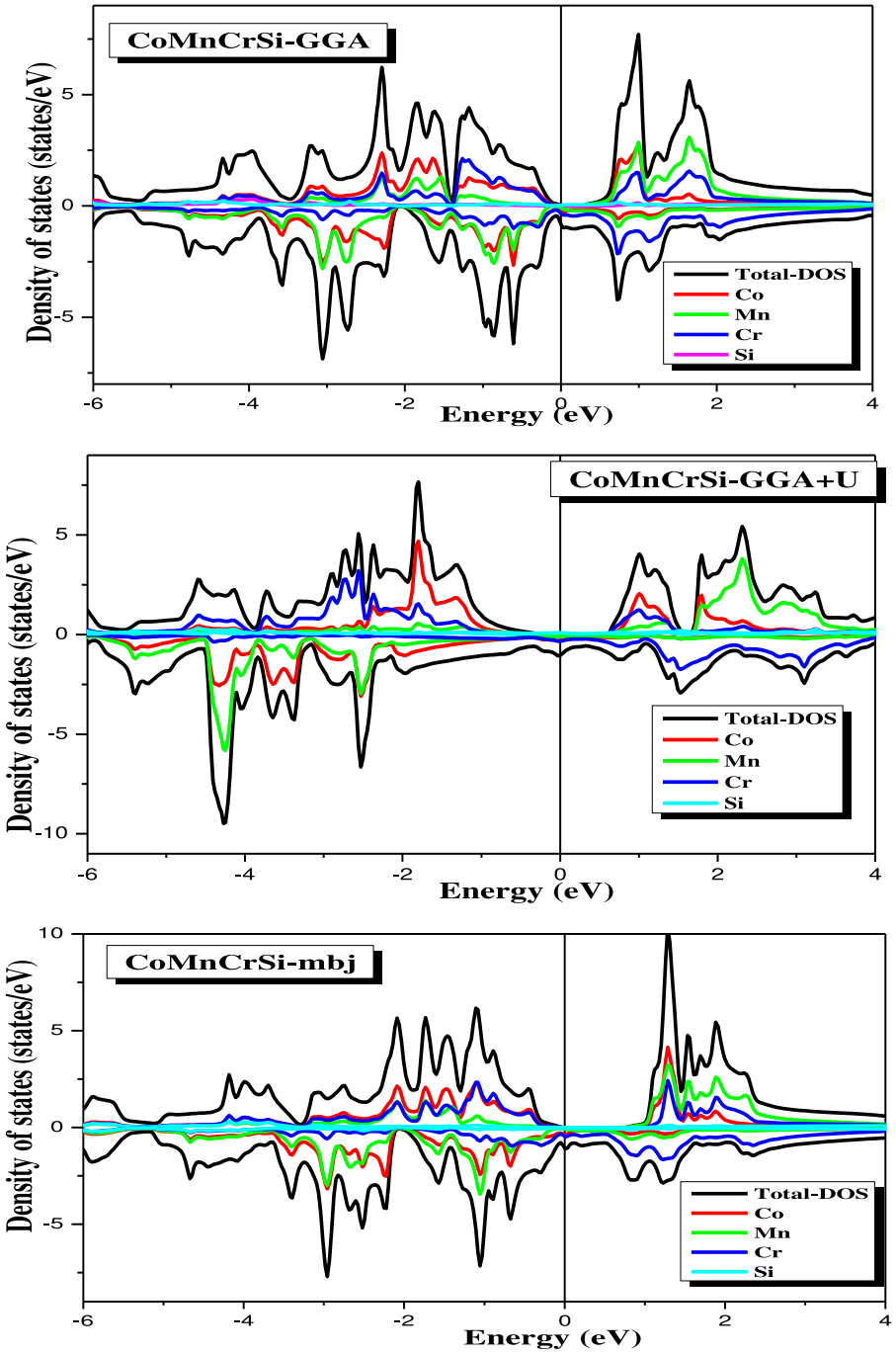

Fig. 4. The density of states for the quaternary Heusler CoMnCrSi computed by GGA, GGA+U and mBJ for spin up and spin down.

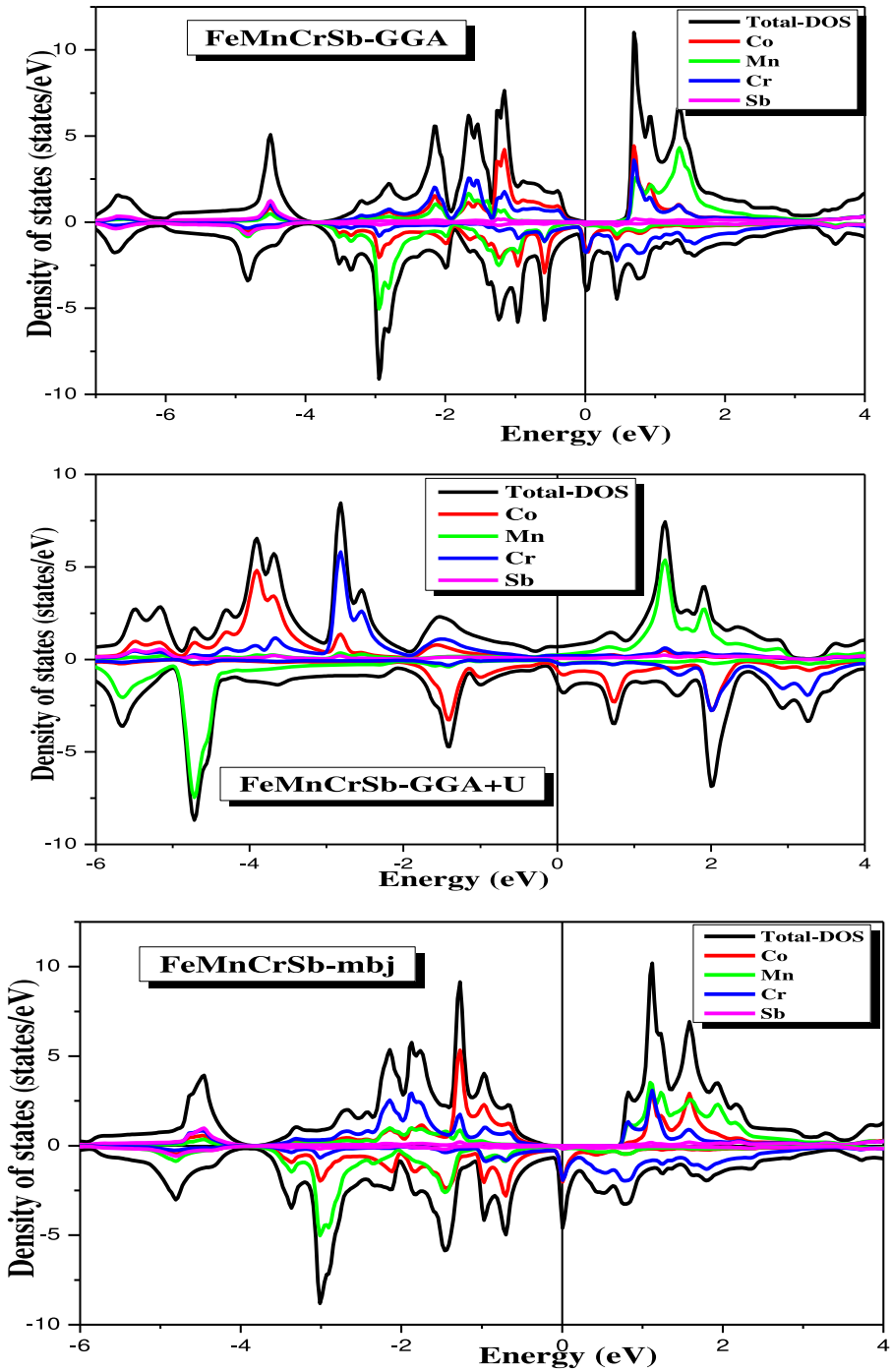

Fig. 5. The density of states for the quaternary Heusler FeMnCrSb computed by GGA, GGA+U and mBJ for spin up and spin down.

Table 4
The band gap for spin up and spin down in CoFeCrAl, CoFeMnSi, CoMnCrSi and FeMnCrSb using GGA, GGA+U and mBJ.

Approach	Spins	CoFeCrAl	CoFeMnSi	CoMnCrSi	FeMnCrSb
E_g (GGA)	down	/	/	/	/
	up	/	/	0.18	0.41
E_g (GGA+U)	down	/	0.32	/	/
	up	0.85	/	0.84	/
E_g (mBJ)	down	/	0.19	/	/
	up	0.97	/	0.76	0.94

Table 5
The magnetic moment by atom and total magnetic moment of CoFeCrAl, CoFeMnSi, CoMnCrSi and FeMnCrSb Heusler using GGA, GGA+U and mBJ.

XX'YY	Approach	μ_X	$\mu_{X'}$	μ_Y	μ_{tot} (μ_B)
CoFeCrAl	GGA	−0.94	−2.38	1.27	−1.89
	GGA+U	−1.70	−3.26	3.09	−1.62
	mBJ	−1.20	−2.62	1.55	−2
CoFeMnSi	GGA	0.92	2.47	0.59	3.92
	GGA+U	1.37	2.91	−3.76	0.42
	mBJ	1.11	2.65	0.44	3.99
CoMnCrSi	GGA	−0.74	−2.41	1.06	−2
	GGA+U	−1.44	−3.76	3.02	−1.99
	mBJ	−0.9	−2.58	1.29	−1.99
FeMnCrSb	GGA	−0.71	−2.9	1.56	−2
	GGA+U	2.61	−4.1	3.69	2.25
	mBJ	−1.01	−3.11	1.98	−1.99

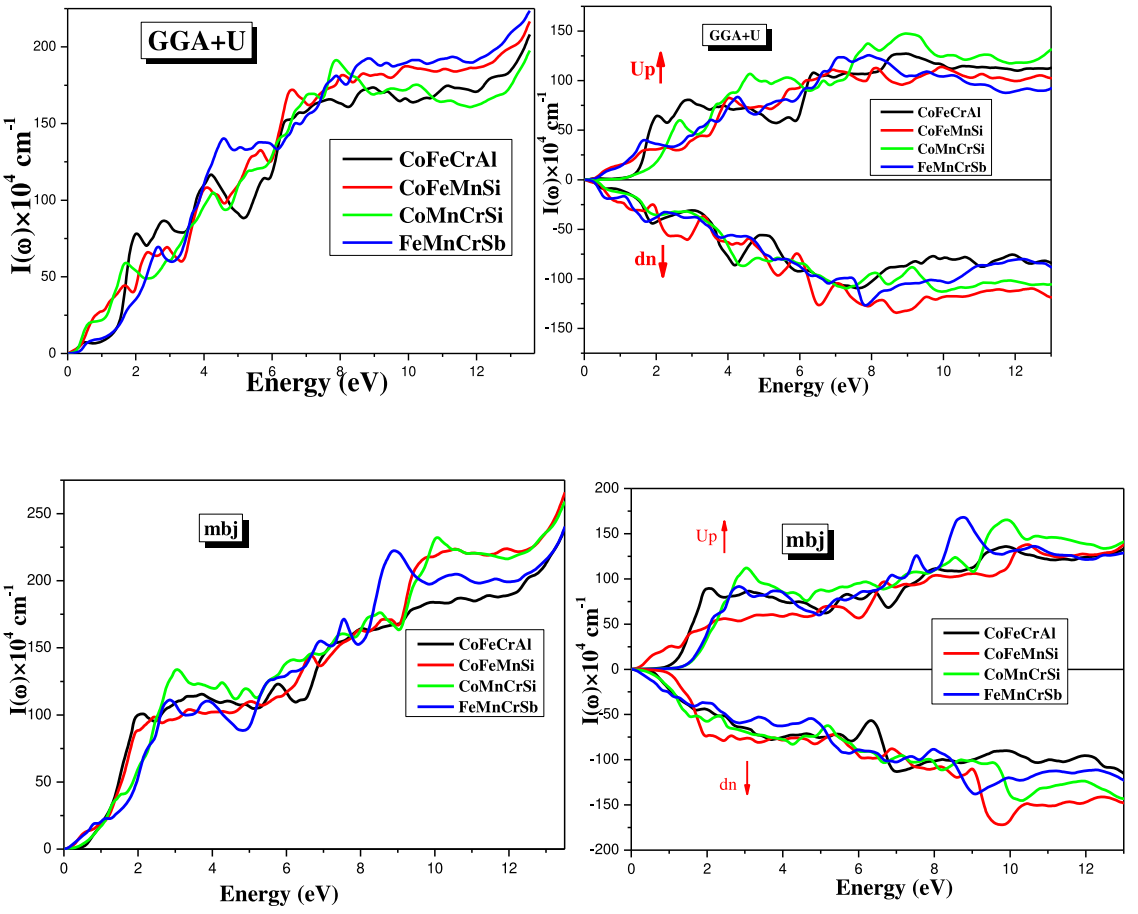

Fig. 6. The absorption coefficient of CoFeCrAl, CoFeMnSi,CoMnCrSi and FeMnCrSb using using GGA+U and mBJ for spin up and spin down.

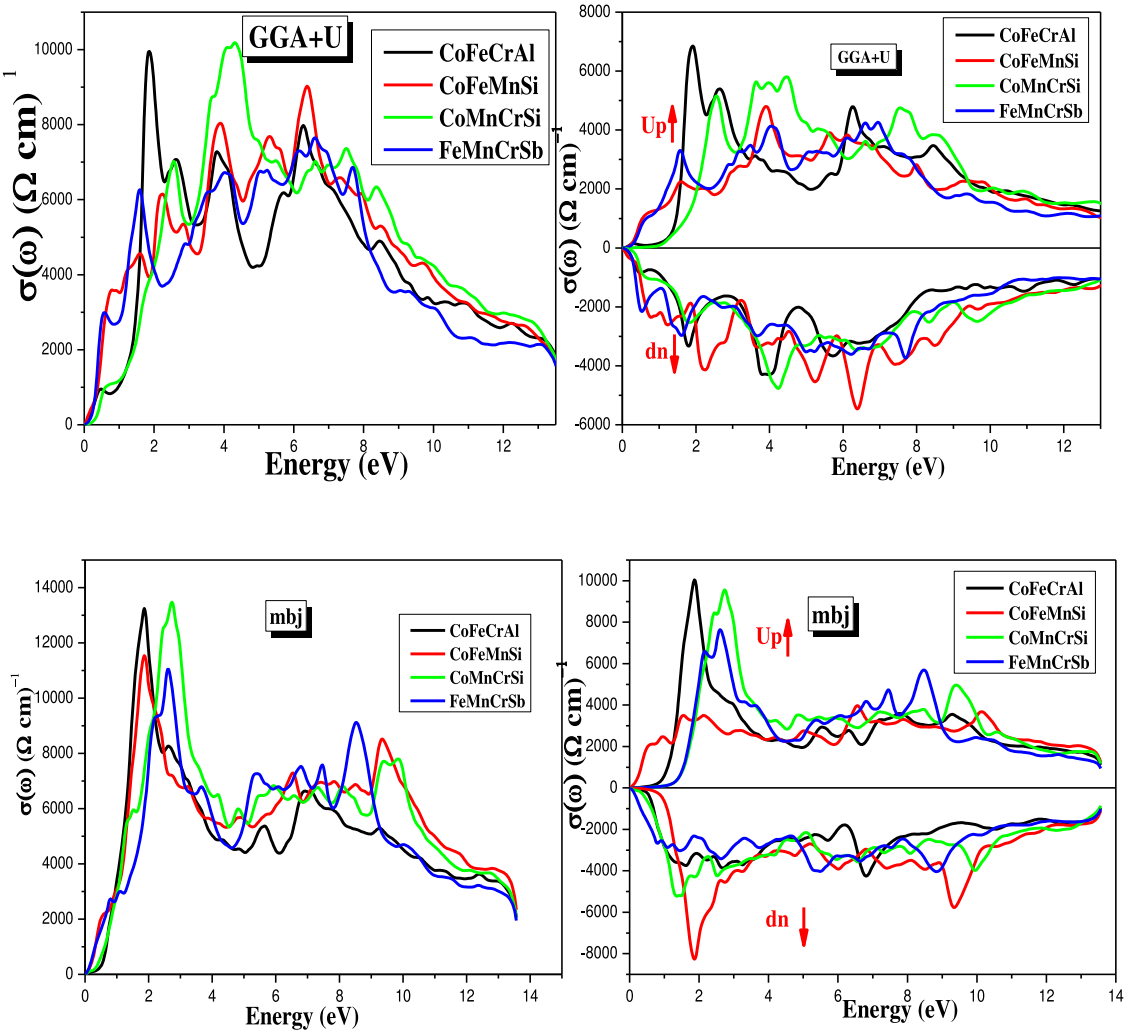

Fig. 7. The optical conductivity of CoFeCrAl, CoFeMnSi, CoMnCrSi and FeMnCrSb using GGA+U and mBJ for spin up and spin down.

Z is the primary group element and X, X', and Y are transition metals [21]. Each Heusler can have three different non-equivalent atomic configurations.

Type 1; X (0, 0, 0), X' (0.25, 0.25, 0.25), Y (0.5, 0.5, 0.5), and Z (0.75, 0.75, 0.75);

Type 2: X (0, 0, 0), X' (0.5, 0.5, 0.5), Y(0.25, 0.25, 0.25), and Z (0.75, 0.75, 0.75);

Type 3: X(0.5, 0.5, 0.5), X' (0, 0, 0), Y (0.25, 0.25, 02.5), and Z (0.75, 0.75, 0.75).

Concerning the CoFeCrAl alloy, the Co, Fe, Cr and Al atoms occupy the positions Co (0, 0, 0), Fe (0.25, 0.25, 0.25), Cr (0.5, 0.5, 0.5) and Al (0.75, 0.75, 0.75). We present in Table 1 the values of $R_{MT}xK_{max}$ of CoFeCrAl, CoFeMnSi, CoMnCrSi and FeMnCrSb, the R_{MT} of each constituent for GGA+U approach. Hubbard's parameter $U_{eff} = 3$ eV is chosen for the all studied transition metals [22,23]. There are eight configurations which depend on the atomic positions of the magnetic materials as well as their spins (up or dn) as shown in Table 2. If we turn the compound by an angle 180 °, config 1 becomes config 5, config 2 becomes config 6, config 3 becomes config 7 and config 4 becomes config 8. We have chosen four more stables cases because of the symmetry. In Fig. 1, we investigate how the unit cell capacity affects the total energy at four ferrimagnetic configurations and one ferromagnetic configuration. CoFeCrAl and CoFeMnSi (CoCrMnSi and CoMnCrSb) are stable at the ferri 1 (ferri 4) configuration. The resistivity of studied quaternary alloys is little sensitive to the temperature, while the electronic conductivity and power factor are proportional to the temperature. We report the equilibrium lattice constant, the bulk modulus and its pressure derivative and the cohesive energy of CoXCrZ (X = Fe, Mn and Z = Al, Si and Sb) and FeMnCrSb quaternary Heusler alloys in Table 3 calculated within GGA and GGA+U approximations. With a lattice constant of 5.95 Å and 6.2184 Å for GGA and GGA+U, the most stable structure is FeMnCrSb because it has the lowest cohesion energy.

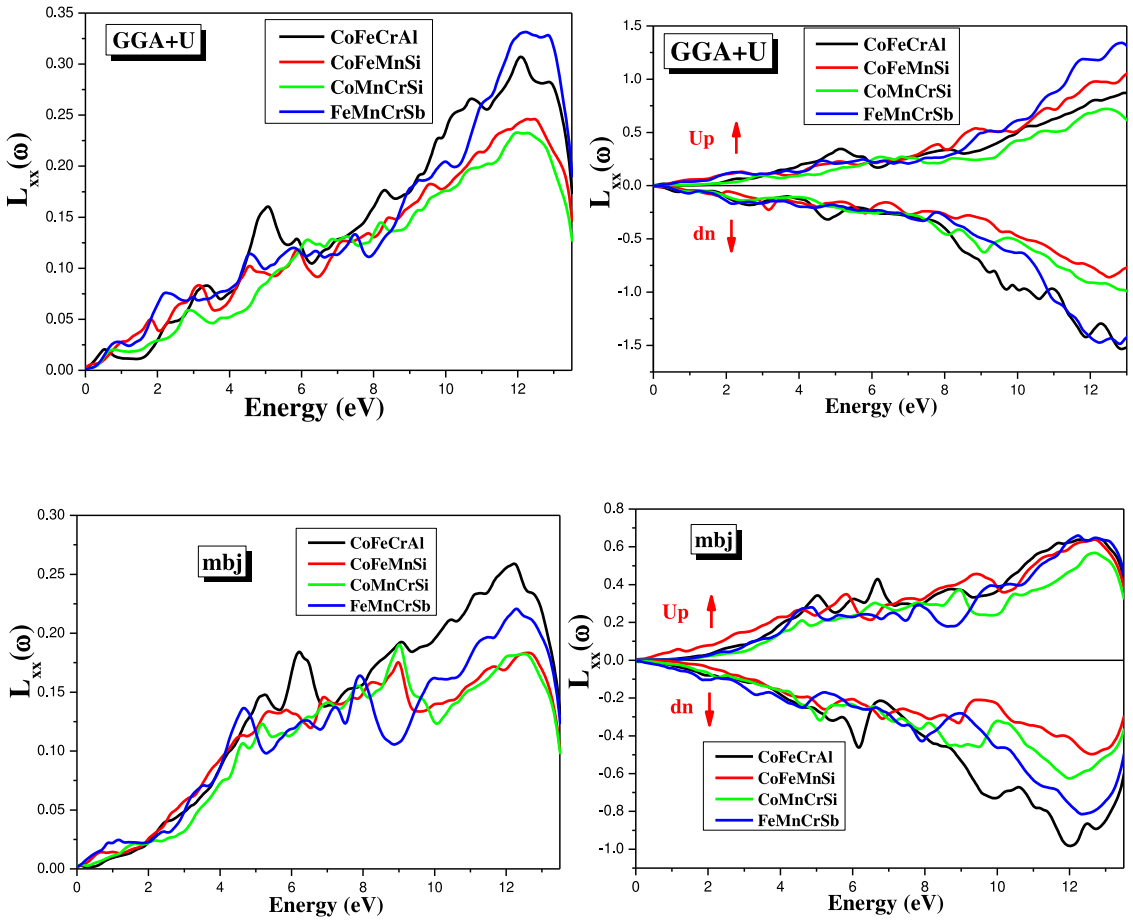

Fig. 8. The energy loss spectra of CoFeCrAl, CoFeMnSi, CoMnCrSi and FeMnCrSb using GGA+U and mBJ for spin up and spin down.

3.2. *Electronic band structures*

The spin direction (↓ and ↑) is used to represent the spin directions of Co, Fe, Mn, and Cr (down and up). The spin-dependent polarized electronic band structure of CoFeCrAl quaternary Heusler for GGA, GGA+U, and mBJ functionals is computed using the equilibrium lattice constants for spin-up (↑) and spin-down (↓) alignment along the high symmetry directions in the first Brillouin zone. We have verified that CoFeCrAl and CoMnCrSi with GGA show a metallic behavior with both spin up and spin down channel. While, CoFeCrAl with GGA+U and CoFeCrAl, with mBJ show a semiconducting behavior for spin up and metallic character for spin down channel. While, CoFeMnSi with GGA, GGA+U and mBJ functionals presents a metallic behavior for both spin up and spin down channel. FeMnCrSb (FeMnCrSb) using GGA, GGA+U and mBJ show a metallic character (a semiconducting character) for spin down (spin up) channel. It is reported that CoFeMnSi (FeMnCrSb) in the GGA+U approach using spin up, the valence band has shifted towards the conduction band (the conduction band has shifted towards the valence band). The elucidation of the manifest ferromagnetism in quaternary Heusler alloys requires the calculation of the total density of states in the majority and minority bands near the Femi level for the type 1 structure. Figs. 2–5 show the density of states behavior for CoFeCrAl, CoFeMnSi, CoMnCrSi and FeMnCrSb quaternary Heusler in the spin up and spin down cases. It can be seen that all spin-polarized band structures have a metallic behavior for the majority spin (spin up), but a band gap at the Fermi level for the minority spin (spin down), except, CoFeCrAl in GGA, CoFeMnSi in GGA and GGA+U and FeMnCrSb in GGA+U present the band gap for spin up and spin down and CoFeMnSi in mBJ has a band gap for spin up and a metallic character for spin down. To ascertain the contribution of various atoms and sites in the valence and conduction bands, the partial density of states must be computed. The upper valence bands of the quaternary Heusler alloys CoFeCrAl, CoFeMnSi, CoMnCrSi, and FeMnCrSb using GGA, GGA+U, and mBJ approximations largely consist of the elements in the spin up and spin down conditions (Co, Fe, Cr, Mn). Except for CoFeCrAl and CoMnCrSi, which use GGA+U, the spin down case has a vacant upper valence band, while the spin up case has an empty valence band for CoFeMnSi, CoMnCrSi, and FeMnCrSb. The ferromagnetism in these quaternary Heusler comes from the coupling between Co-Cr, Co-Mn and Co-Fe states. In the spin-up region, there is a band gap between the valence and conduction bands, whereas in the spin-down region, a tiny state of the valence band is present at E_F, resulting in a metallic character in that channel. Because E_F exists between VBM and CBM with no overlapping of states, it is apparent that all of these alloys are semiconductors in spin up. However, because to the current conditions at E_F, spin down is metallic. The energy

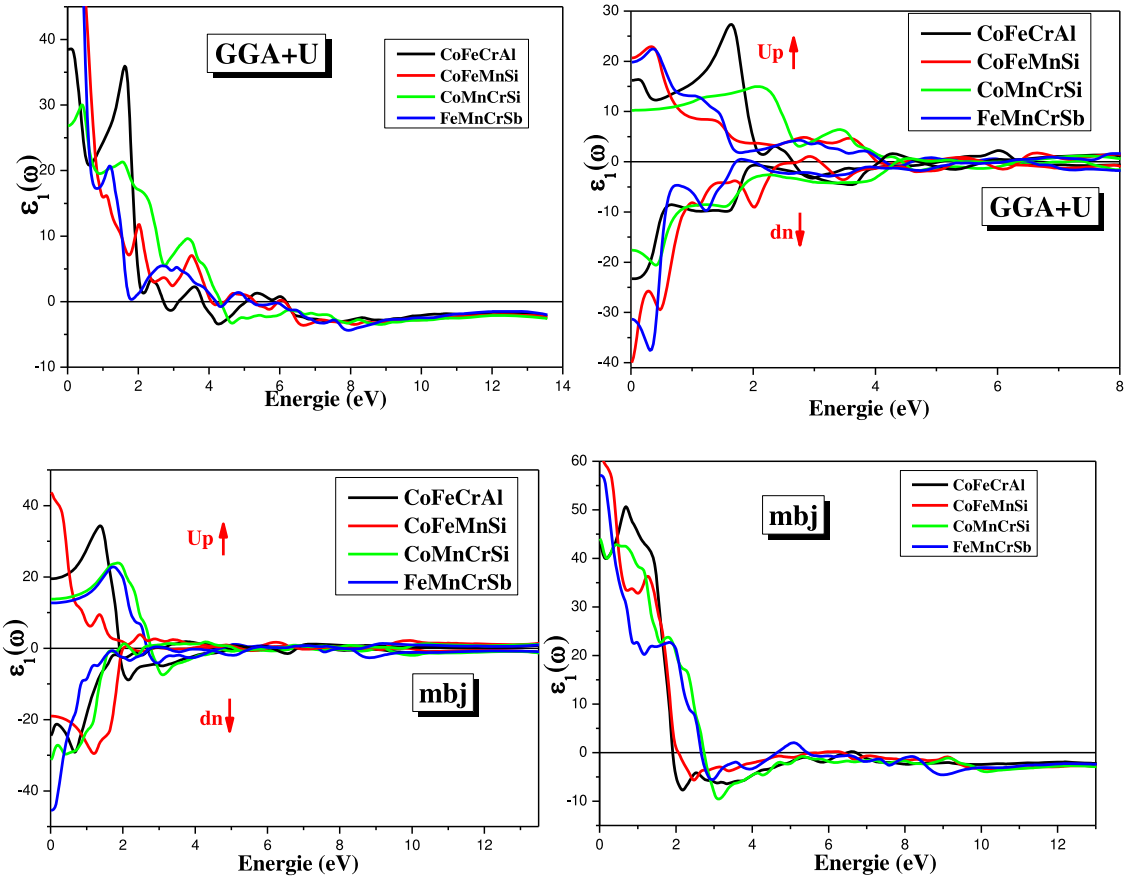

Fig. 9. The real part of the dielectric function as a function of energy for CoFeCrAl, CoFeMnSi, CoMnCrSi and FeMnCrSb using GGA+U and mBJ for spin up and spin down.

differential between the valence and conduction bands is known as the band gap.

3.3. Magnetic properties

Table 4 provides the spin-down FM energy gap G_{gmin} and HM gap G_{hm} for CoFeCrAl, CoFeMnSi, CoMnCrSi, and FeMnCrSb based on the GGA, GGA+U, and mBJ approximations. The gap G_{hm} is the difference between the minima of the electronic band structure in the spin-down channel of the conduction band and the Fermi level, whereas the gap G_{gmin} is the energy difference between the top of the valence band and the conduction states surrounding the Fermi level. Table 5 displays the computed total and local magnetic moments of a number of sites for CoFeCrAl, CoFeMnSi, CoMnCrSi, and FeMnCrSb in the ferromagnetic state using GGA, GGA+U, and mBJ. In the quaternary Heusler alloys CoFeCrAl and CoFeMnSi, it is noted that Co and Fe sites generate permanent local magnetic moments. While, Co and Mn sites contribute to the magnetism in CoMnCrSi and the contribution in FeMnCrSb comes from Fe and Mn sites. The magnetic moment due to the Cr atom is in the spin up direction in all studied alloys, except for the case of CoFeMnSi alloy in the GGA+U approximation, where it is oriented in the spin down direction. The magnetic moment of Cr is antiparallel to the Fe, Co and Mn moments for CoFeCrAl, CoMnCrSi, and FeMnCrSb alloys. The magnetic moment of Mn is parallel to the Co and Fe moments for CoFeMnSi alloy, except for the GGA+U case, where it is antiparallel. The total magnetic moment is mostly derived from Fe, Co, Cr, and Mn atoms, with minor contributions from Al, Si, and Sb sites, and it is lowered by Co-Cr and Co-Mn hybridization.

3.4. Optical properties

For CoFeCrAl, CoFeMnSi, CoMnCrSi, and FeMnCrSb, the GGA+U and mBJ approximations were used to calculate the absorption coefficient, optical conductivity, electron energy loss, real and imaginary part of the dielectric function, reflectivity, refractive index, and extinction coefficient for in-plane [100] crystallographic direction in the spin up and spin down cases. These variables are isotropic for a cubic phase material. The extinction coefficient and absorption coefficient are linked directly by:

$$\alpha(\omega) = \frac{2\omega}{C}k$$

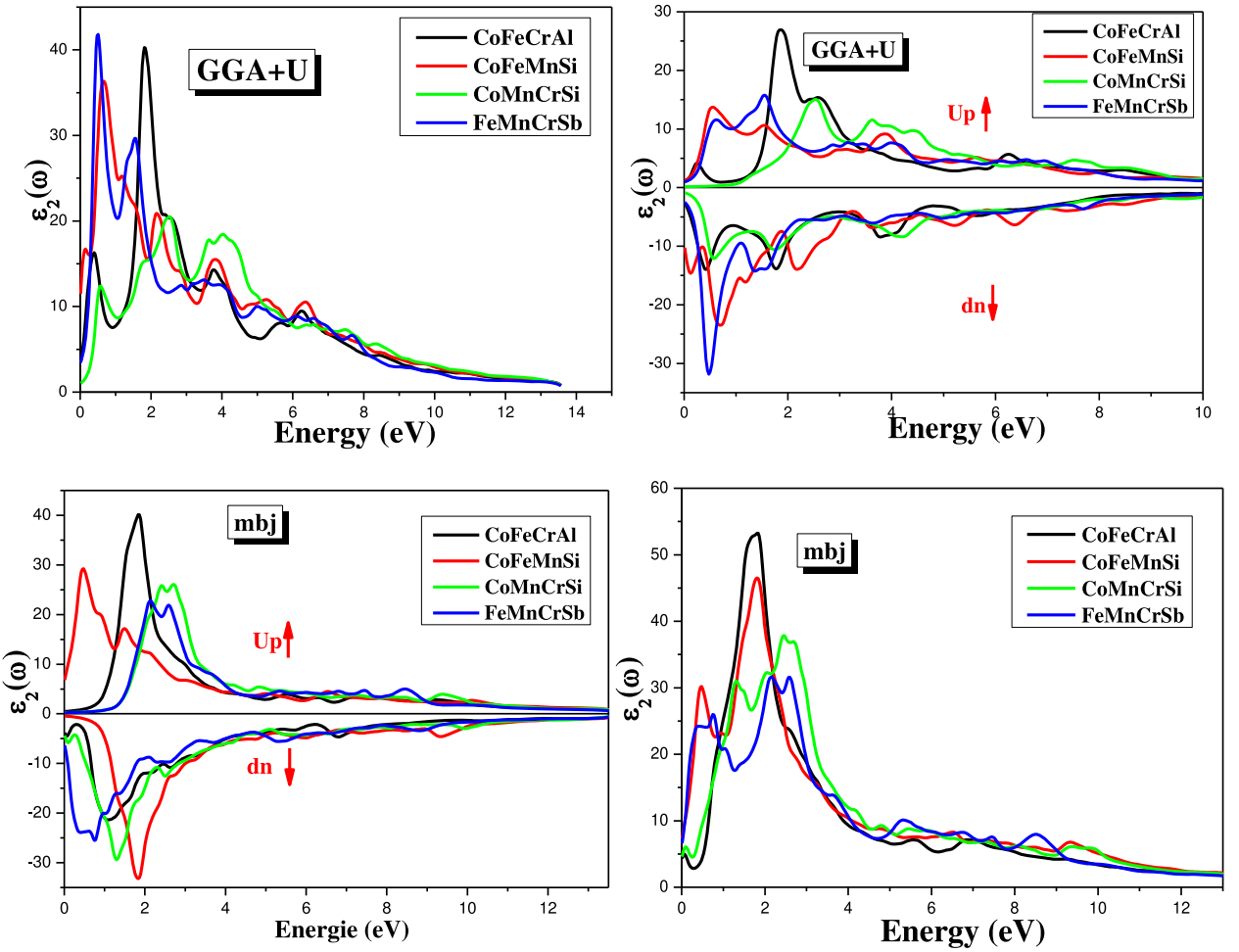

Fig. 10. The imaginary part of the dielectric function as a function of energy for CoFeCrAl, CoFeMnSi, CoMnCrSi and FeMnCrSb using GGA+U and mBJ for spin up and spin down.

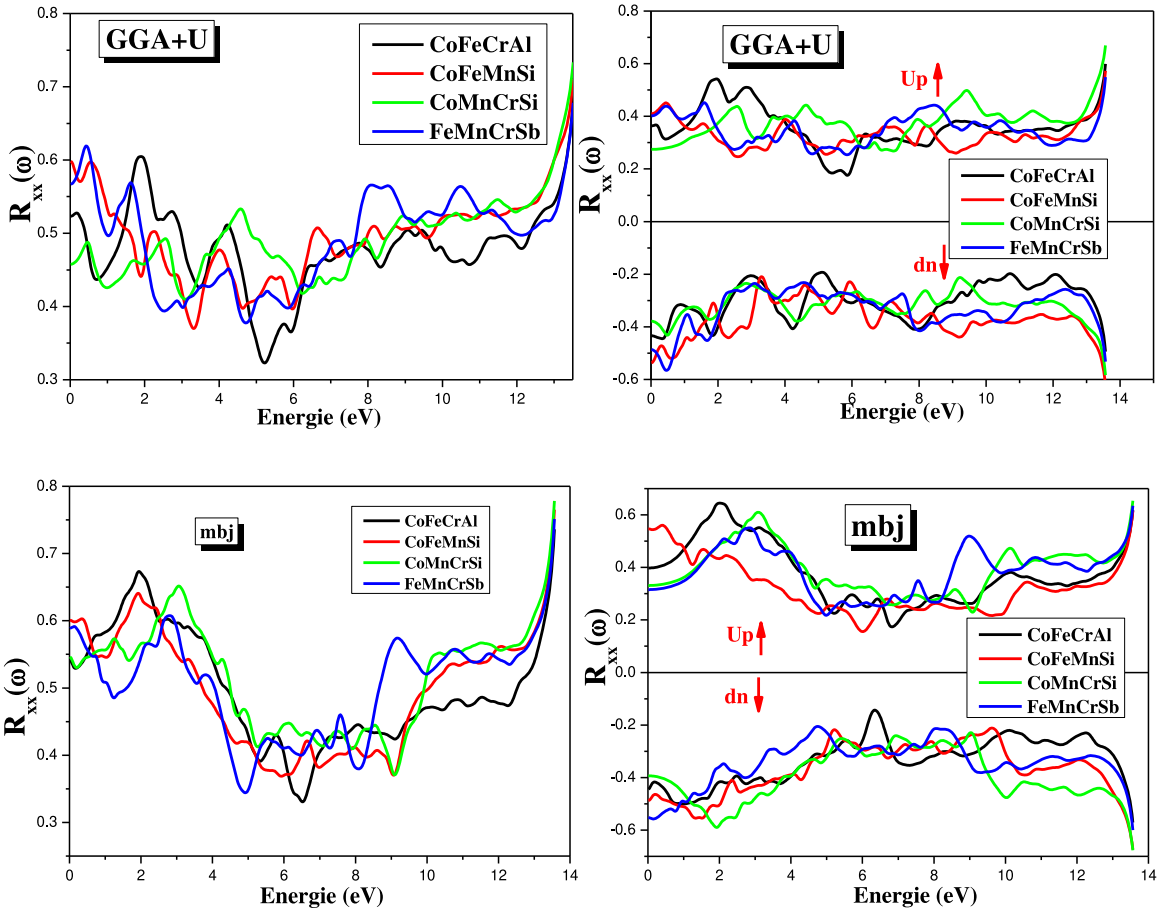

Fig. 11. The reflectivity spectra of CoFeCrAl, CoFeMnSi, CoMnCrSi and FeMnCrSb using GGA+U and mBJ for spin up and spin down.

The imaginary part of the dielectric function is associated to the optical conductivity by:

$$\sigma(\omega) = \frac{\omega}{4\pi}\varepsilon_2(\omega)$$

N = n + ik, where n(ω) is the refractive index and k(ω) is the extinction coefficient, is the formula for the complex refractive index N. Refractive index and extinction coefficient are directly related to the following expressions: The complex refractive index N is directly related to the dielectric constant$N = \sqrt{\varepsilon}$.

$$n(\omega) = \frac{\sqrt{\varepsilon_1^2(\omega) + \varepsilon_2^2(\omega)} + \sqrt{\varepsilon_1(\omega)}}{\sqrt{2}}$$

$$\kappa(\omega) = \frac{\sqrt{\varepsilon_1^2(\omega) + \varepsilon_2^2(\omega)} - \sqrt{\varepsilon_1(\omega)}}{\sqrt{2}}$$

As a function of refractive index and extinction coefficient, the reflectivity is provided by;

$$R(\omega) = \frac{(n-1)^2 + \kappa^2}{(n+1)^2 + \kappa^2}$$

The real and hypothetical components of the dielectric function are connected to the electron energy loss.

$$L(\omega) = \frac{\varepsilon_2(\omega)}{[\varepsilon_1^2(\omega) + \varepsilon_2^2(\omega)]}$$

The impact of photon energy on the aforementioned parameters is shown in Figs. 6-13. The absorption coefficient value is located between (100 and 200) x10^4 cm^{-1}, it presents a high value in the mBJ approach. All spectra show a similar shape in GGA+U and mBJ approaches. They are symmetrical with respect to the energy axis in the cases of spins up and down. Between 4 and 10 eV of UV energy is absorbed by these substances. The amount of absorption validates the candidature of CoFeCrAl, CoFeMnSi, CoMnCrSi, and

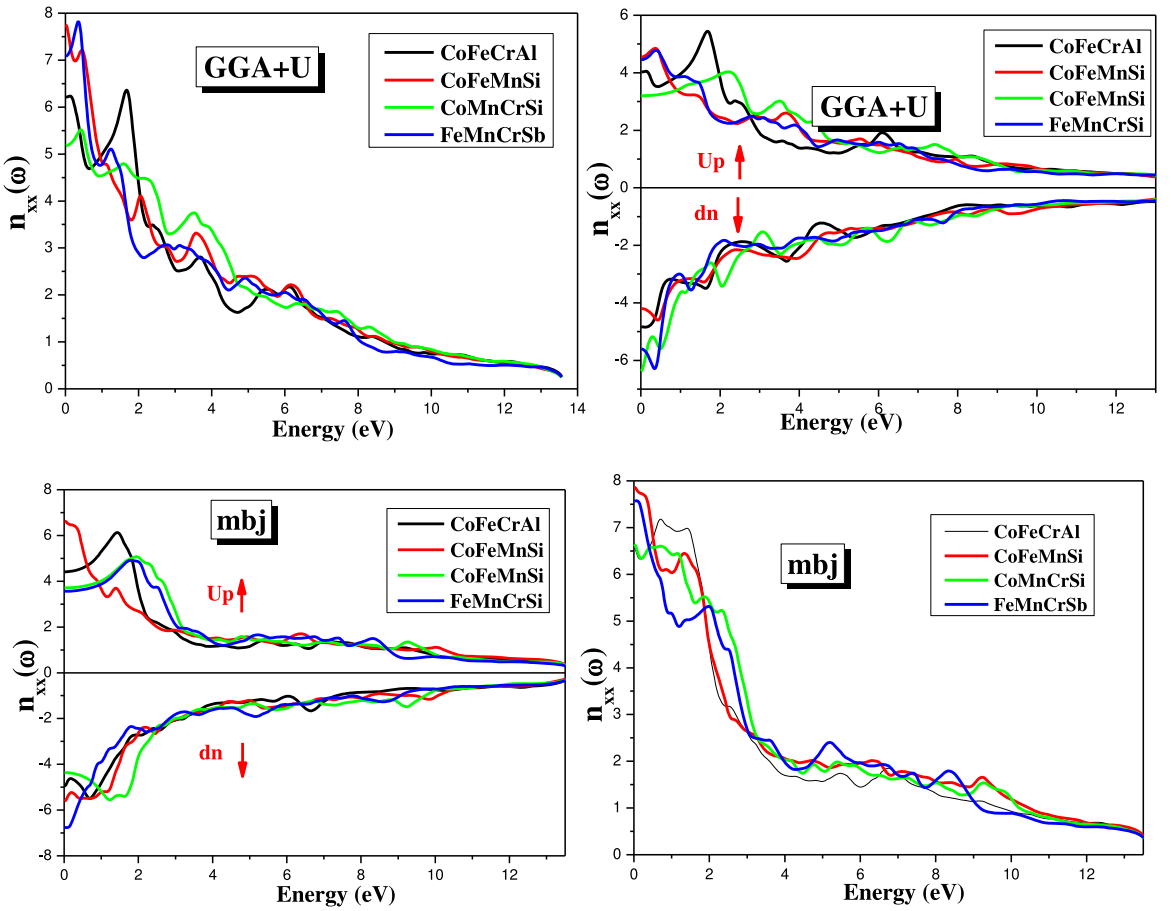

Fig. 12. The refractive index as a function of energy for CoFeCrAl, CoFeMnSi, CoMnCrSi and FeMnCrSb using GGA+U and mBJ for spin up and spin down.

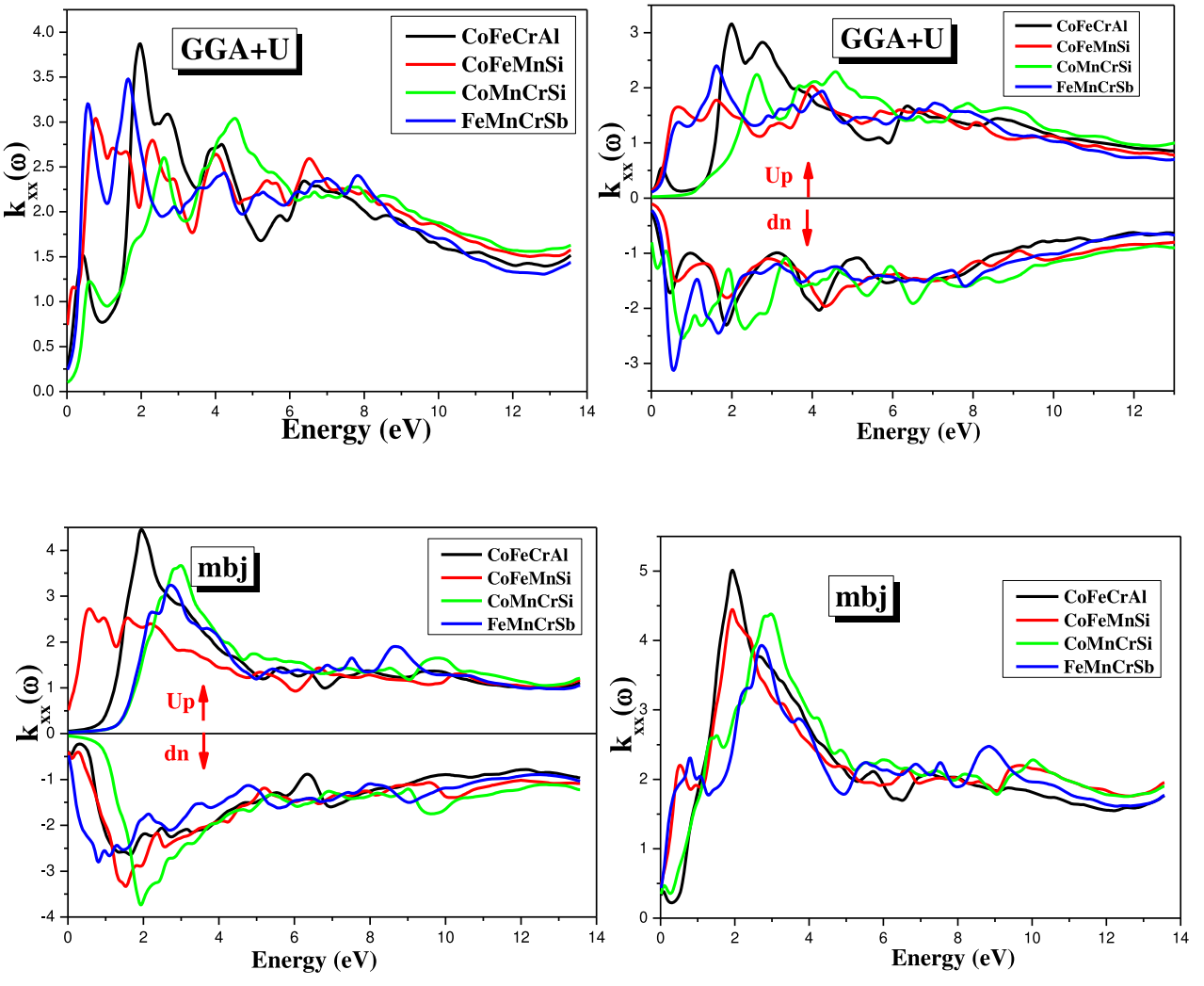

Fig. 13. The extinction coefficient as a function of energy for CoFeCrAl, CoFeMnSi, CoMnCrSi and FeMnCrSb using GGA+U and mBJ for spin up and spin down.

Table 6
The static dielectric constant and static refractive index $\varepsilon_1(0)$ and n (0) of CoFeCrAl, CoFeMnSi et CoMnCrSi and FeMnCrSb Heusler calculated using GGA+U and mBJ.

Heusler	ε_1 (0)		n (0)	
	GGA+U	mBJ	GGA+U	mBJ
CoFeCrAl	38.48	42.97	6.21	4.41
CoFeMnSi	59.66	61.69	4.54	6.62
CoMnCrSi	26.81	44.06	3.20	3.71
FeMnCrSb	50.14	57.12	4.45	3.56

FeMnCrSb as absorber for photovoltaic devices. For the quaternary Heusler CoFeCrAl, CoFeMnSi, CoMnCrSi, and FeMnCrSb crystals, we investigate the impact of photon energy on optical conductivity under incidence along in-plane [100] crystallographic direction. The flat in the conductivity spectrum using GGA+U and mBJ is estimated to be 10000 $\Omega^{-1}cm^{-1}$ and 13000 $\Omega^{-1}cm^{-1}$ and positioned in the range 1.5 eV – 8 eV. The optical conductivity is more important in CoFeCrAl and CoMnCrSi, especially in the spin up case. The crystal's photonic band structure is connected to the characteristics of the energy-loss spectrum. The electron's contact with the crystal results in energy loss. The extreme ultraviolet light area is the only place where the Heusler alloys CoFeCrAl, CoFeMnSi, CoMnCrSi, and FeMnCrSb experience electron energy loss. The maximum energy loss is about 30 % and 25% for GGA+U and mBJ, it is reported that the spin up reduces the loss. The real part of the dielectric function aids in foretelling the material's nonlinear optical behavior. The static dielectric constant values of CoFeCrAl, CoFeMnSi, CoMnCrSi, and FeMnCrSb Heusler alloys for in-plane [100] direction are reported in Table 6. The spin reduces the static dielectric constant value. The absorptive capability of such a material is represented by the fictitious portion of the dielectric function. The intense peaks in the in-plane [100] direction of dielectric function are located between 0.5 eV and 2 eV (0.5 eV – 2.5 eV) for GGA+U (mBJ) approach, which suggest inter band transition, and the photon emission is not possible in these materials. The static refractive index values of CoFeCrAl, CoFeMnSi, CoMnCrSi, and FeMnCrSb quaternary Heusler alloys are reported in Table 6 for in-plane [100] direction using GGA+U and mBJ approximations. The material's refractive index gauges how transparent it is to incoming spectrum radiation. When photons pass through a substance and when atoms are bound together by covalent bonds, the refractive index becomes more significant. It can be seen that the spin reduces the static refractive index. The reflectivity of a material is a measurement of its capacity to reflect radiation. In the area of extremely ultraviolet light, the reflectivity of Heusler alloys made of CoFeCrAl, CoFeMnSi, CoMnCrSi, and FeMnCrSb achieves many maxima and minima, and the spin increases the reflectivity. In reality, the reflectivity is constrained by interdiffusion, oxidation, and thermal stability. The extinction coefficient measures the energy loss of radiation passing through a medium. The mBJ approximation gives high extinction coefficient than GGA+U. The spin reduces the extinction coefficient for in-plane [100] direction in both approaches. The studied compounds had a small energy gap, which is one of the features interested in studying photovoltaic. by studying the optical conductivity in the field of 2 – 6 electron volts, and also the absorption is strong for higher energy. We can consider these compounds as good within the energies shown in the figures and use them in solar panels.

3.5. *Thermoelectric properties*

The transport properties of CoXCrZ (X = Fe, Mn, and Z = Al and Si) and FeMnCrSb quaternary Heusler are investigated as a function of the chemical potential for three distinct temperatures (300 K, 600 K, and 800 K). The thermoelectric material has lattice stability, a mechanical thermal as well a high figure of merit (ZT). Thermal transport coefficients such as Seebeck coefficient, electrical condctivity, electronic thermal conductivity, figure of merite, power factor as a function of chemical potential at three fixed temperatures T = 300 K, 600 K and 800 K for CoFeCrAl, CoFeMnSi, CoMnCrSi, and FeMnCrSb Heusler alloys are displayed in Figs. 14-17. The amplitude of an induced thermoelectric voltage in response to a temperature difference across a material is measured by the Seebeck coefficient, also known as thermoelectric sensitivity of a material. For half-metallic materials, total Seebeck coefficient is evaluated by using the two-current model as follows [24] $S = (S_{\uparrow}\sigma_{\uparrow} + S_{\downarrow}\sigma_{\downarrow})/\sigma_{total}$, where $S_{\uparrow}(S_{\downarrow})$ and $\sigma_{\uparrow}(\sigma_{\downarrow})$ are the Seebeck coefficients and electrical conductivities for the spin-up (spin-down) channel, respectively. The $\sigma_{total} = (\sigma_{\uparrow} + \sigma_{\downarrow})$ represents the total electrical conductivity. For the spin down case using mBJ approach, the increase in temperature from 300 K to 800 K reduces the Seebeck coefficient in CoFeMnSi from (0.0004 to 0.00022) μV/K. For the spin up case, the increase in temperature from 300 K to 800 K reduces the Seebeck coefficient in CoFeCrAl, FeMnCrSi and FeMnCrSb from (0.0005 to 0.00022) μV/K, from (0.0013 to 0.0005) μV/K and from (0.0014 to 0.0005) μV/K. For two-parabolic bands, one for electrons and another for holes, the Seebeck coefficient is computed. The Seebeck coefficient of certain material depends on its electronic band structure. The dispersion of conduction band edge near the Fermi level decreases, while the dispersion of valence band edge around the Fermi level increases. This phenomenon induces a small effective mass of CBM and small effective mass of VBM. A small effective mass at the band edge will induce a small Seebeck coefficient [25]. The negative value of the S suggests the presence of n-type charge carriers (electrons), while the positive value suggests the presence of p-type carriers (holes) [26]. The location of the optimum chemical potential is determined by the material's kind and operating temperature. The Seebeck coefficient is slightly asymmetric as a result of the mass difference between electrons and holes. The thermoelectric figure of merit, ZT, evaluates the rivalry between thermal transmission and electrical transport (power factor) (total thermal conductivity). For the spin up case, the increase in temperature from 300 K to 800 K reduces the figure of merite in CoFeCrAl, CoMnCrSi and FeMnCrSb from (0.9 to 0.7) at (0 to 0.25) Ry, (0.95 to 0.9) at (0.25 to 0.8)Ry and (1 to 0.9) at (0 to 0.5) Ry. For the spin down case using mBJ approach, the increase in temperature from 300 K to 800 K reduces the figure of merit in CoFeMnSi from (0.8 to 0.65) at (0 to 0.2) Ry. For the

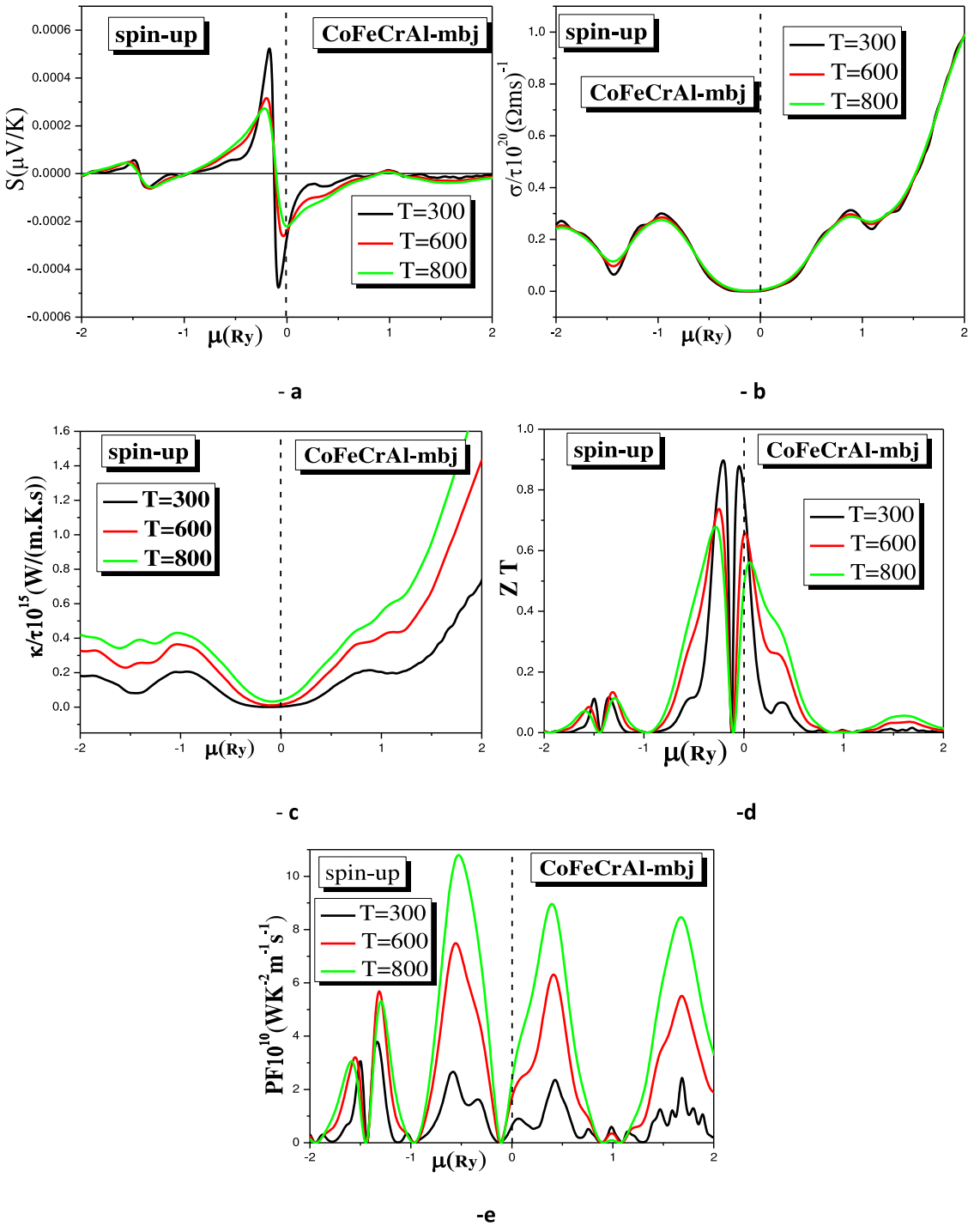

Fig. 14. The Seebeck coefficient (a), electrical condctivity (b), electronic thermal conductivity (c), figure of merite (d), Power factor (e) as a function of chemical potential at three fixed temperatures T = 300 K, 600 K and 800 K for CoFeCrAl using mBJ.

identical two-band model, the maximum ZT is determined. The highest ZT is calculated using the same two-band model. We utilized a constant relaxation time estimate ($\tau = 10^{-13}$ s for both bands) to calculate ZT, which implies a constant phonon lattice thermal conductivity. At room temperature, calculations are performed. Each Heusler has two ZT peaks, one for n-type and the other for p-type. As p-type and n-type, ZT's two peaks have similar values. As a result, these materials have the same thermoelectric efficiency whether they are p-type or n-type. The total electrical conductivity of the p-type increases at a faster rate than the n-type. In the case of CoFeCrAl, where $\sigma/\tau = (10^{20})$ $(\Omega ms)^{-1}$, the rise is greater. It's also worth noting that overall electrical conductivity curves are less

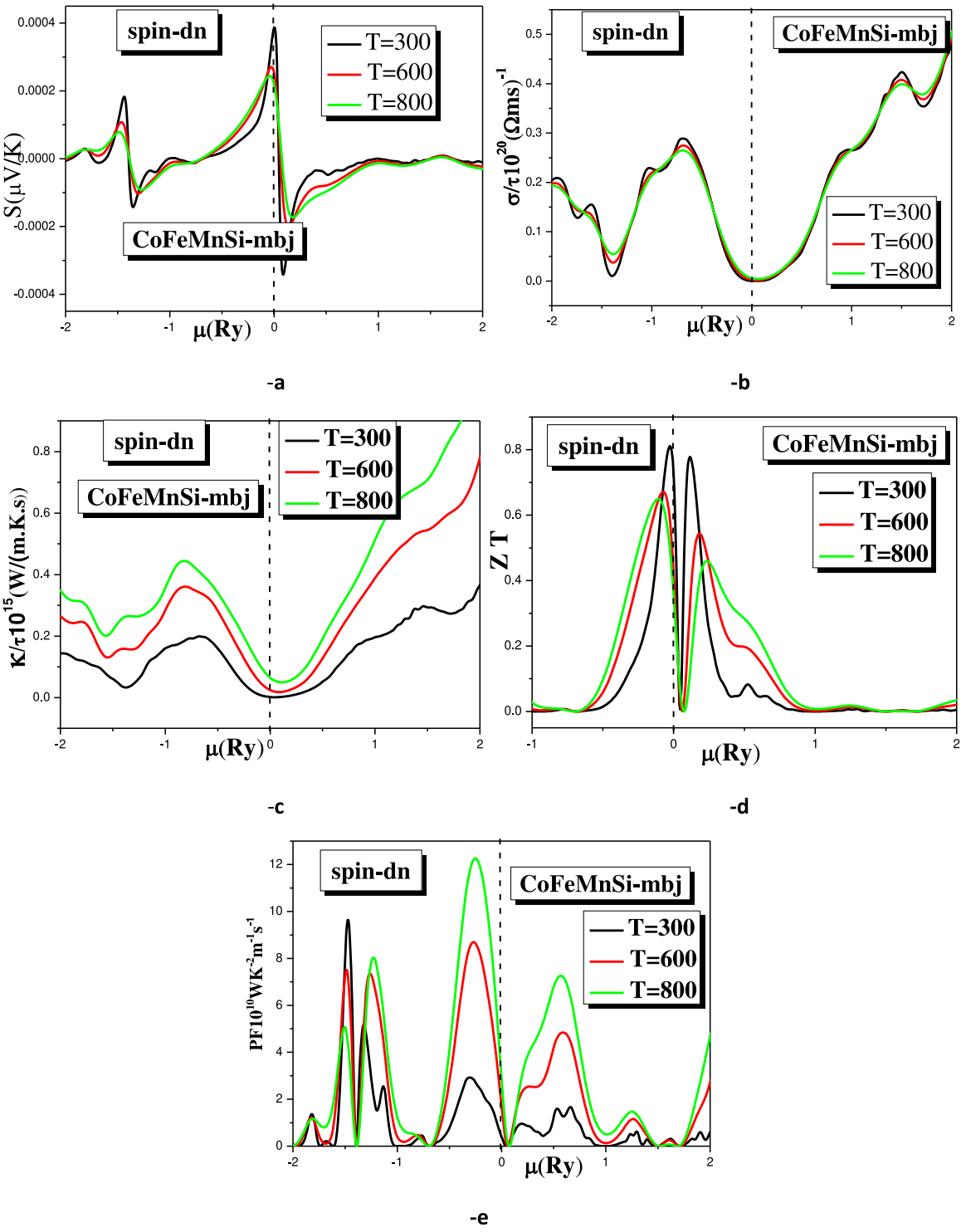

Fig. 15. The Seebeck coefficient (a), electrical condctivity (b), electronic thermal conductivity (c), figure of merite (d), Power factor (e) as a function of chemical potential at three fixed temperatures T = 300 K, 600 K and 800 K for CoFeMnSi using mBJ.

temperature sensitive. For CoFeMnSi, CoMnCrSi and FeMnCrSb, $\sigma/\tau = (0.45 - 0.5)(10^{20})$ $(\Omega ms)^{-1}$. The total electronic conductivity of the p-type increases at a faster rate than the n-type. It's also worth noting that total electronic conductivity curves are temperature sensitive. The total electronic conductivity increases with increasing temperature. The ratio of the real power absorbed by the load to the visible power flowing in the circuit is known as the power factor of a system. The n-type has a bigger increase in power factor values

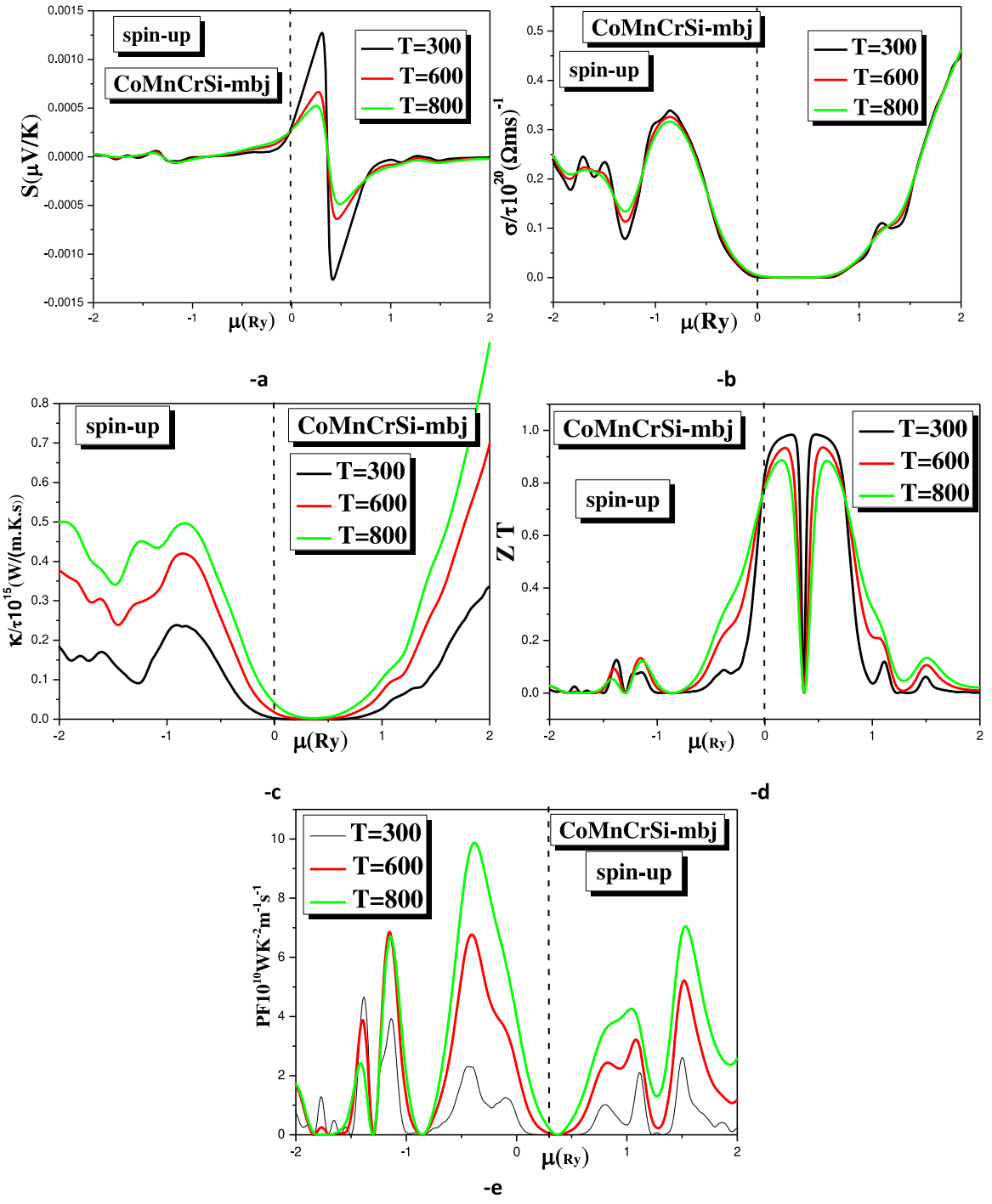

Fig. 16. The Seebeck coefficient (a), electrical condctivity (b), electronic thermal conductivity (c), figure of merite (d), Power factor (e) as a function of chemical potential at three fixed temperatures T = 300 K, 600 K and 800 K for CoMnCrSi using mBJ.

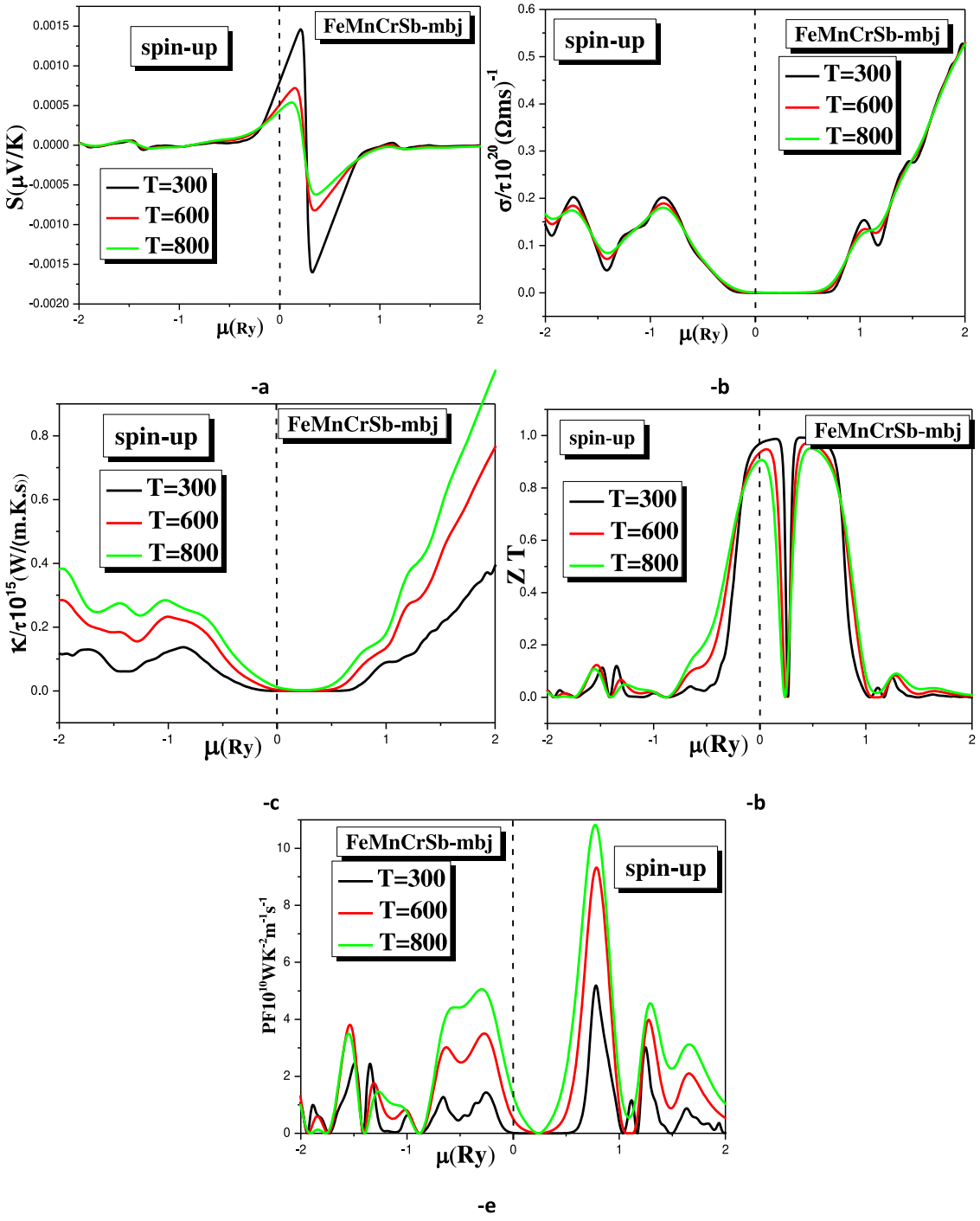

Fig. 17. The Seebeck coefficient (a), electrical condctivity (b), electronic thermal conductivity (c), figure of merite (d), Power factor (e) as a function of chemical potential at three fixed temperatures T = 300 K, 600 K and 800 K for FeMnCrSb using mBJ.

than the p-type. It's also worth noting that power factor curves are temperature sensitive. The power factor increases with increasing temperature.

4. Conclusion

We studied the most stable quaternary Heusler structure in three distinct atomic configurations (type-1, type-2 and type-3). Using cohesion energy calculations, the stability of these quaternary Heusler alloys has been studied. The half-metallicity of these quaternary Heusler is intimately tied to the magnetic atom configurations in the Heusler structure. The 3d electrons of the Fe, Co, Mn, and Cr atoms are primarily responsible for the magnetization of these quaternary Heusler. In these materials, one spin possesses a band gap and a limited density of states at the Fermi level. The electronic structure of Heusler alloys is governed by the degree of structural organization and distribution of the atoms in the crystal lattice. FeMnCrSb, CoFeCrAl, CoFeMnSi, CoMnCrSi With high Curie temperatures, Heusler alloys exhibit SGS behavior, making them viable substitutes for diluted magnetic semiconductors. The increase in temperature for the spin up case reduces the figure of merite and increases the total electronic conductivity in these quaternary Heusler. The resistivity of studied quaternary alloys is little sensitive to the temperature, while the electronic conductivity and power factor are proportional to the temperature.

Declaration of Competing Interest

The authors declare that they have no known competing financial interests or personal relationships that could have appeared to influence the work reported in this paper.

Acknowledgements

We would like to thank Taif University Research Supporting Project number (TURSP-2020/63), Taif University, Taif, Saudi Arabia.

References

[1] A. Kundu, S. Ghosh, R. Banerjee, S. Ghosh, B. Sanyal, New quaternary half-metallic ferromagnets with large Curie temperatures, Sci. Rep. 7 (2017) 1803–1818, https://doi.org/10.1038/s41598-017-01782-5.
[2] J. He, M. Amsler, Y. Xia, S.S. Naghavi, V.I. Hegde, S. Hao, S. Goedecker, V. Ozoliņš, C. Wolverton, Ultralow thermal conductivity in full Heusler semiconductors, Phys. Rev. Lett. 117 (2016) 046602–046606, https://doi.org/10.1103/PhysRevLett.117.046602.
[3] R. Haleoot, B. Hamad, Ab initio investigations of the structural, electronic, magnetic, and thermoelectric properties of CoFeCuZ (Z = Al, As, Ga, In, Pb, Sb, Si, Sn) quaternary Heusler alloys, J. Electron. Mater 48 (2019) 1164–1173, https://doi.org/10.1007/s11664-018-6833-1.
[4] Y. Ohnuma, M. Matsuo, S. Maekawa, Spin transport in half-metallic ferromagnets, Phys. Rev. B 94 (18) (2016) 184405–184410, https://doi.org/10.1103/PhysRevB.94.184405.
[5] J. Drews, U. Eberz, H. Schuster, Optische Untersuchungen an farbigen intermetallischen phasen, J. Less-Common Met. 116 (1986) 271–278, https://doi.org/10.1016/0022-5088(86)90235-3.
[6] X. Dai, G. Liu, G.H. Fecher, C. Felser, Y. Li, H. Liu, New quarternary half metallic material CoFeMnSi, J. Appl. Phys 105 (2009) 1–3, https://doi.org/10.1063/1.3062812.
[7] N. Arıkan, A. İyigör, A. Candan, S. Uğur, Z. Charifi, H. Baaziz, G. Uğur, Electronic and phonon properties of the full-Heusler alloys X2YAl (X = Co, Fe and Y = Cr, Sc): a density functional theory study, J. Mater. Sci. 49 (2014) 4180–4190, https://doi.org/10.1007/s10853-014-8113-7.
[8] T. Dietl, H. Ohno, F. Matsukura, J. Cibert, D. Ferrand, Zener model description of ferromagnetism in zinc-blende magnetic semiconductors, Science 287 (2000) 1019–1022, https://doi.org/10.1126/science.287.5455.1019.
[9] M. Torrichi, A. Belfar, A. Mokeddem, Ferromagnetism in (X, Y)-Codoped 4H-GaN Polytype X = Na and Mg, Y = Na and Mg: Ab Initio Study, J. Supercond. Novel Magn. 32 (2019) 335–340, https://doi.org/10.1007/s10948-018-4718-4.
[10] L. Bainsla, A.L. Mallick, M. Manivel Raja, A.A. Coelho, A.K. Nigam, D.D. Johnson, A. Alam, K.G. Suresh, Origin of spin gapless semiconductor behavior in CoFeCrGa: theory and experiment, Phys. Rev. B 92 (2015) 045201–045205, https://doi.org/10.1103/PhysRevB.92.045201.
[11] Y. Jin, R. Skomski, P. Kharel, S.R. Valloppilly, D.J. Sellmyer, Effect of disorder on the resistivity of CoFeCrAl films, AIP Adv. 7 (2017) 055834–055840, https://doi.org/10.1063/1.4978591.
[12] K. Özdoğan, E. Sasıoğlu, I. Galanakis, Slater-Pauling behavior in LiMgPdSn-type multifunctional quaternary Heusler materials: half-metallicity, spin-gapless and magnetic semiconductors, J. Appl. Phys. 113 (2013) 193903–193908, https://doi.org/10.1063/1.4805063.
[13] L. Bainsla, A.I. Mallick, A.A. Coelho, A.K. Nigam, B.S.D.C.S. Varaprasad, Y.K. Takahashi, A. Alam, K.G. Suresh, K. Hono, High spin polarization and spin splitting in equiatomic quaternary CoFeCrAl Heusler alloy, J. Magn. Magn. Mater. 394 (2015) 82–86, https://doi.org/10.1016/j.jmmm.2015.05.095.
[14] M. Torichi, Theoretical Study of Electronic and Thermoelectric Properties of Sodium Doped 4H-GaN Polytype, AJRT 5 (1) (2021) 49–56.
[15] L. Bainsla, A.I. Mallick, M. Manivel Raja, A.K. Nigam, B.S.D.Ch.S. Varaprasad, Y.K. Takahashi, A. Alam, K.G. Suresh, K. Hono, Spin gapless semiconducting behavior in equiatomic quaternary CoFeMnSi Heusler alloy, Phys. Rev. B 91 (2015) 104408–104414, https://doi.org/10.1103/PhysRevB.91.104408.
[16] K. Schwarz, P. Blaha, G.K.H. Madsen, Electronic structure calculations of solids using the WIEN2k package for material sciences, Comp. Phys. Commun. 147 (2002) 71–76, https://doi.org/10.1016/S0010-4655(02)00206-0.
[17] J.P. Perdew, K. Burke, M. Ernzerhof, Generalized gradient approximation made simple, Phys. Rev. Lett. 77 (1996) 3865–3868, https://doi.org/10.1103/PhysRevLett.77.3865.
[18] A.D. Becke, E.R. Johnson, A simple effective potential for exchange, J. Chem. Phys. 124 (2006) 221101–221105, https://doi.org/10.1063/1.2213970.
[19] V.I. Anisimov, O. Gunnarsson, Density-functional calculation of effective Coulomb interactions in metals, Phys. Rev. B 43 (1991) 7570–7574, https://doi.org/10.1103/PhysRevB.43.7570.
[20] M.A. Ghebouli, T. Chihi, B. Ghebouli, M. Fatmi, Study of the structural, elastic, electronic and optical properties of lead free halide double perovskites Cs2AgBiX6 (X= Br, Cl) 56 (2018) 323–330, https://doi.org/10.1016/j.cjph.2018.01.004.
[21] P. Wang, J.B. Xia, H.B. Wu, Electronic structures, magnetic properties and strain effects of quaternary Heusler alloys FeMnCrZ (Z = P, As, Sb, Bi, Se, Te), J. Magn. Magn. Mater. 490 (2019) 165490–165499, https://doi.org/10.1016/j.jmmm.2019.165490.
[22] S. Das, M.D.I. Bhuyan, First-principles calculation of the electronic and optical properties of Gd2FeCrO6 double perovskite: effect of Hubbard U parameter, J. Mater. Res. Technol. 13 (2021) 2408–2418, https://doi.org/10.1016/j.jmrt.2021.06.026.
[23] S.I. Dudarev, G.A. Botton, S.Y. Safrasov, C.J. Humphreys, A.P. Sutton, Electron-energy-loss spectra and the structural stability of nickel oxide: an LSDA+U study, Phys. Rev. B 57 (1998) 1505–1509, https://doi.org/10.1103/PhysRevB.57.1505.

[24] H.J. Xiang, D.J. Singh, Suppression of thermopower of NaxCoO2 by an external magnetic field: Boltzmann transport combined with spin-polarized density functional theory, Phys. Rev. B 76 (2007) 195111–195116, https://doi.org/10.1103/PhysRevB.76.195111.
[25] J. Li, Y. Wang, G. Zhang, H. Yin, D. Chen, W. Sun, B. Shi, Z. Cheng, Seeking large Seebeck effects in LaX(X = Mn and Co)O3/SrTiO3 superlattices by exploiting high spin-polarized effects, Phys. Chem. Chem. Phys. 21 (2019) 14973–14983, https://doi.org/10.1039/C9CP02486G.
[26] J. Li, G. Zhang, C. Peng, W. Wang, J. Yang, Y. Wang, Z. Cheng, Magneto-Seebeck effect in $Co_2FeAl/MgO/Co_2FeAl$: first-principles calculations, Phys. Chem. Chem. Phys. 21 (10) (2019) 5803–5812, https://doi.org/10.1039/C8CP07697A.